Article

The outdoor field test of the 4T III-V on Si tandem PV module and its energy yield modeling

Kenji Araki [1]*, Hiroki Tawa [2], Hiromu Saiki [2], Yasuyuki Ota [3], Kensuke Nishioka [2] and Masafumi Yamaguchi [1]

[1] Toyota Technological Institute, Nagoya 468-8511, Japan
[2] Faculty of Engineering, University of Miyazaki, Miyazaki 889-2192, Japan
[3] Organization for Promotion of Tenure Track, University of Miyazaki, Miyazaki 889-2192, Japan
* Correspondence: cpvkenjiaraki@toyota-ti.ac.jp; Tel.: +81-52-8091830

Featured Application: This technology is expected to be applied to high-performance photovoltaic applications like zero-emission buildings and light-weight aerospace.

Abstract: The outdoor field test of the 4-terminal III-V on Si tandem photovoltaic module (specifically, InGaP/GaAs on Si) was investigated and performance model, considering spectrum change affected by fluctuation of atmospheric parameters, was developed and validated. The 4-terminal III-V on Si tandem photovoltaic module had about 40 % advantage in seasonal performance loss compared with standard InGaP/GaAs/InGaAs 2-terminal tandem photovoltaic module. This advantage is expanded in (subarctic zone) < (temperate zone) < (subtropical zone).

Keywords: photovoltaic; energy yield; output forecasting; aerosol optical depth; precipitable water; incident angle

1. Introduction

High-efficiency power or energy conversion is the typical research target of photovoltaic technology. However, it is also known through field experience and theoretical analysis considering spectrum fluctuation that the photovoltaic system that wins the efficiency-race does not always perform the best in the real world [1-4].

Currently, Si solar cell has commonly prevailed in the market. The best efficiency of the Si that was confirmed testing laboratories is 26.7% [5], and the theoretical limit is 29.43% [6]. For further improvement of efficiency, multi-junction or tandem configuration is preferred. The principles of multi-junction cells were suggested in 1955 [7] and investigated in 1960 [8]. The significant progress was triggered by liquid-phase, and the vapor-phase epitaxy brought AlGaAs/GaAs multi-junction cells in the 1980s, with tunnel junctions [9] and metal interconnections [10-12]. At that moment, it was predicted that the power-conversion efficiency of multi-junction solar cells would reach close to 30% [13], but this was not achieved because of difficulties with high-performance, stable tunnel junctions [14] as well as oxygen-related defects in the AlGaAs at that time [15]. The break-through was a high-performance, stable tunnel junctions with a double-hetero (DH) structure [16]. Later on, InGaP was introduced for the top cell [17], and as a result, it was finally achieved to 29.5% efficiency by a 0.25 cm^2 GaInP/GaAs two-junction cell [18]. More recently, 37.9% efficiency and 38.8% efficiencies have been achieved with InGaP/GaAs/InGaAs 3-junction cells [19] and with a 5-junction cell [20].

On-Si tandem solar cells use the widely-used Si solar cell as the bottom junction of the tandem solar cell. Because the technology of Si solar cells is well-established, the production cost of the solar cell is expected to reduce, at least, the one to the substrate or the bottom junction [21]. The III-V/Si (III-V on Si) 3-junction and 2-junction tandem solar cells right now exhibit excellent efficiency with 35.9% [22] and 32.8% [22]. That of the perovskite/Si 2-junction tandem solar cells is 28.0% [23]. That of CdZnTe/Si 2-junction tandem solar cell is 16.8% [24]. That of GaAs nano-wire/Si 2-junction tandem solar cell is 11.4% [25]. The III-V/Si tandem solar cell has the best efficiency among them. Related to

Preprints (www.preprints.org) | NOT PEER-REVIEWED | Posted: 2 March 2020 doi:10.20944/preprints202003.0028.v1

this III-V/Si tandem solar cell technologies, several module technologies, including a partial concentrator module [26]. The tested power conversion efficiency of a pair of InGaP/GaAs partial concentrator cell on Si, including optical loss of the concentrator optics, was 27.1% [27]. The partial concentrator module, also using InGaP/GaAs partial concentrator cell on Si and designed for automobile application, showed 21.5% module efficiency [28]. The non-concentrating module using InGaP/GaAs cell on InGaAs by 4T configuration showed 31.17% [1, 29].

Regardless of the material type combined with Si bottom junction, mismatching loss by the spectrum change will be a big issue [30-35]. Four-terminal (4T) tandem cells were designed so that the output of the Si cell and other top junctions were taken independently, thus robust to the spectrum change. In the case of III-V/Si three-junction solar cells that are frequently considered as an excellent candidate for the high-efficiency solar cells, the output terminal from the top cell comes from two-junction III-V solar cells, and the top two-junction cell is still susceptible to spectrum change. Therefore, a long-term field test of the module using III-V/Si 4T solar cells is essential to the validation of the use of this configuration. Currently, the best efficiency confirmed by the third-party is 33.3% [36].

2. Methods

The purpose of our work is to develop an accurate method of predicting the performance of photovoltaic modules using tandem 4T solar cells, considering spectrum variation. The base model of the spectrum is Bird's model [37]. Bird's model only covers the clear sky days, and we expanded it to cover all-climate roughly [38]. This new spectrum model and the response of the tandem module was validated by the long-term (multiple years) measurement of the performance of the module [38].

2.1. Device configuration

The fundamental difference of 2T and 4T configuration is that the former one connects entire sub-cells all in series, and the latter divides the circuit into two pieces using two-pairs of output lead, namely, four-terminal (Figure 1). Each pair of leads can be connected to two independent loads so that each 2T output can be controlled by independent MPPT (maximum power point tracking). There are two advantages. One is less loss in spectrum mismatching because the shorter-wavelength zone and longer-wavelength zone are connected independent loads. Another is more flexibility in the design of the solar cell. In this particular case, the 4T configuration uses Si to the bottom sub-cell and III-V two-junction cell in the top sub-cell. Both sub-cell technologies are well-established, and it is not necessary to consider various constraints of the integration into one-piece (typically monolithic growth) solar cells.

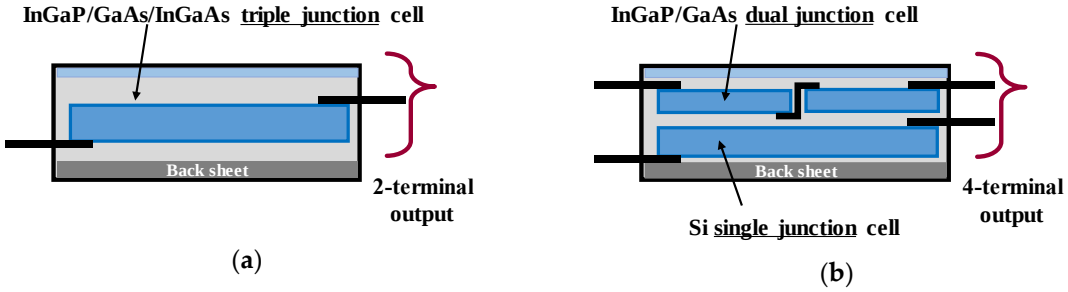

Figure 1. Measured 4T III-V/Si module and its solar cell structure: (**a**) Description of measured 4T III-V/Si module, 2 + 1 junctions (right) with comparison to the 2-terminal III-V 3-junction module. Note that the number of junctions is the same; (**b**) Spectro-radiometers installed at the University of Miyazaki [38].

2.2. Measurement system

The field test was done at the University of Miyazaki. The details of the measurement setup can be found in our recent publication of Applied Sciences [38], as shown in Figure 2.

Preprints (www.preprints.org) | NOT PEER-REVIEWED | Posted: 2 March 2020 doi:10.20944/preprints202003.0028.v1

The sub-module with InGaP/GaAs two-junction solar cell on Si solar cell was fabricated by SHARP and installed at the University of Miyazaki along with a 2T three-junction module (InGaP/GaAs/InGaAs). The output characteristics of these PV modules were measured using an I-V curve tracer. Pyranometers were installed on 25° (EKO MS-602) and 35° (EKO MS-411) inclined platforms to measure global irradiance. A pyranometer was also installed on a two-axis sun-tracking (EKO MS-602) to measure global normal irradiance. Measurements were carried out every 3 min from 5:30 a.m. to 6:30 p.m. The solar spectrum was measured using spectro-radiometers (EKO MS-711, MS-712). They were installed on 35° inclined platforms. Measurements were made every 10 min from 5:00 a.m. to 8:00 p.m.

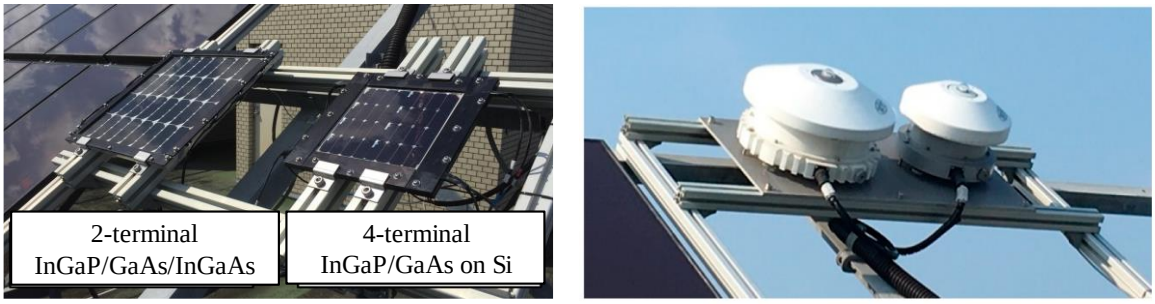

(**a**) (**b**)

Figure 2. Measured 4T III-V/Si module and its solar cell structure: (**a**) Description of measured 4T III-V/Si module, 2 + 1 junctions (right) with comparison to the 2-terminal III-V 3-junction module. Note that the number of junctions is the same; (**b**) Spectro-radiometers installed at the University of Miyazaki [38].

2.3. Spectrum model

The performance model we used was identical to the one we used to analyze the PV module using the 2T configuration [38]. We called it an MS2E model (Miyazaki Spectrum-to-Energy method). Let us describe a rough flow of the analysis and the model.

First, we need to define the solar spectrum. The spectrum we assumed was a linear combination of the spectrum of the clear sky condition and that of the overcasting condition [38]. The spectrum of the overcasting condition was assumed that the solar power was lost just by absorption, corrected by the solid angle of the sky affected by the slope angle of the module. Then, the solar spectrum is approximated as Equation (1) and Equation (2).

$$I_\lambda = f I_{1\lambda} + (1 - f) I_{2\lambda} \quad (1)$$

$$f = \frac{DNI}{\int_{300\,nm}^{4000\,nm} I_{d\lambda} d\lambda} \quad (2)$$

where, I_λ is the global spectral irradiance using our spectrum model considering all-weather at a wavelength (W/m²nm), f is the weather correction factor defined by Equation (2), $I_{1\lambda}$ is the global spectral irradiance calculated using Bird's spectrum model [37] at a wavelength (W/m²nm), $I_{2\lambda}$ is the global spectral irradiance calculated using a new spectrum model assuming full cloud cover at a wavelength (W/m²nm), DNI is the direct normal irradiance, and $I_{d\lambda}$ is the direct normal spectral at a wavelength (W/m²nm). The spectrum calculated by this model, with contrast to Bird's model is shown in Figure 3 [38]. Note that the Bird's spectrum model was improved by considering atmospheric parameter variability and cloud conditions. The Y-axis corresponds to normalized by integrated spectral irradiance to evaluate the shape of the solar spectrum. The black trend line is the measured global solar spectrum. The gray trend line is the reference spectrum in AM 1.5G. The red trend line and the blue trend line are the estimated global solar spectrum using the MS2E method and Bird's model considering only air mass, respectively. In the wintertime, atmospheric parameters are close to those under the standard conditions, so that the estimated solar spectrum approaches to the reference AM1.5G spectrum. In the summertime, the aerosol density often becomes smaller than

Preprints (www.preprints.org) | NOT PEER-REVIEWED | Posted: 2 March 2020 doi:10.20944/preprints202003.0028.v1

that of the standard value, and the precipitable water becomes larger. The short-wavelength region of the solar spectrum becomes fat, and the long-wavelength region becomes thin. During the cloudy days, the influence of cloud appears in the short-wavelength region of the solar spectrum so that the long-wavelength region drops.

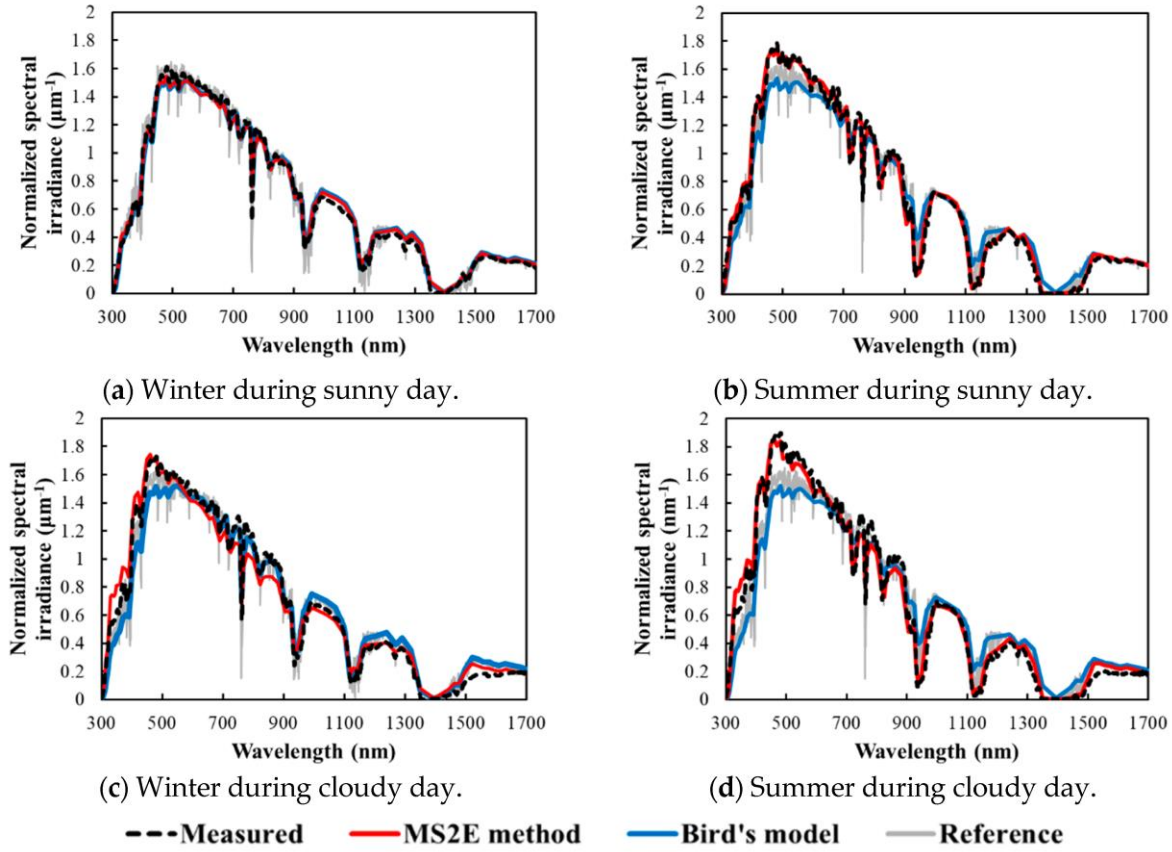

Figure 3. Comparison with measured and estimated values (Bird's model and MS2E model) of global irradiances tilted at 35° [38].

2.4. Performance model

The power output of the module is the product of the short-circuit current, open-circuit voltage, and fill factor (*FF*). First, *FF* was calculated by the ratio of the spectrum mismatching—specifically, generating a correlation chart between calculated *FF* and the ratio of mismatching at first; then, a general trend of these two parameters was fitted to the parabolic curve so that the *FF* is represented as the function of the spectrum-mismatching index. The short-circuit current can be calculated as the integral of the product of the spectral irradiance and spectral efficiency of the module, which can be calculated from the external quantum efficiency affected by spectrum mismatching. The angular characteristics in the photon absorption were measured in advance. The detailed calculation procedure was identical to our previous work [38].

We also need to solve the complicated coupling of spectrum and angles. The key parameters are atmospheric parameters that are dependent on each other. For example, different incident angle modifier and different orientation lead to a diverse mixture of direct and diffused sunlight. The atmospheric parameters were calculated by the spectrum, using a data-fitting calculation called the Bird's model [39-40] at the University of Miyazaki [41]. The developed model for the analysis of non-concentrating solar cells is given in Figure 4 [1]. The nonlinear effect result from distributed effects often seen in III-V (especially concentrator cells) was not considered [42-43].

Preprints (www.preprints.org) | NOT PEER-REVIEWED | Posted: 2 March 2020 doi:10.20944/preprints202003.0028.v1

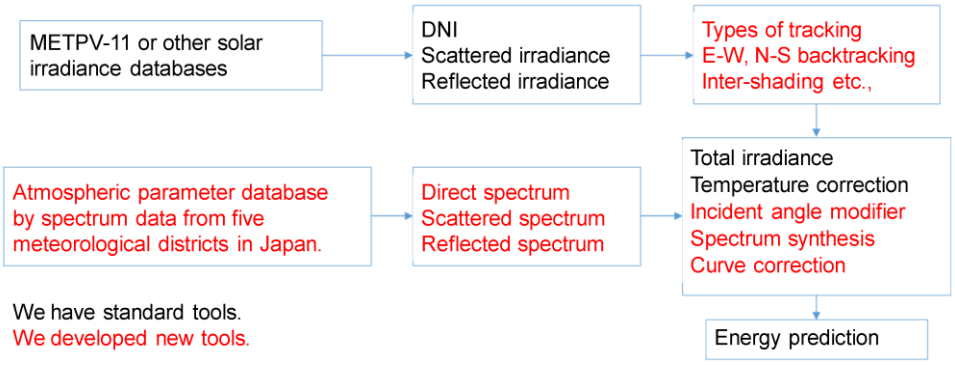

Figure 4. Modeling performance of the non-concentrating multi-junction solar cells considering the complicated spectrum and angle interaction [1]. In this study, we only considered the flat plate, so that correction to the curved surface in the integrated tool was not applied.

3. Results

First, we examined our performance model (MS2E model) that could be applied to the PV module using 4T tandem cells. We monitored the module performance in every 3 minutes from 05:30 to 18:30 on January 3, 2019. The slope angle was 35°. The location of the test site at the University of Miyazaki was N31.83°, E131.42°. The result of the measurement and the validation result is shown in Figure 5 and Table 1. The output trend in Figure 5 was decomposed to InGaP/GaAs top cell and Si bottom cell, namely, we applied independent MPPT (maximum power point tracking) search to each pair of the terminals. The predicted output of the 4T tandem module using our MS2E performance model supported by the all-climate spectrum model (Equation (1) and (2)) matched well. It was also shown that the accuracy in prediction of the daily energy yield is within plus or minus 2% of error.

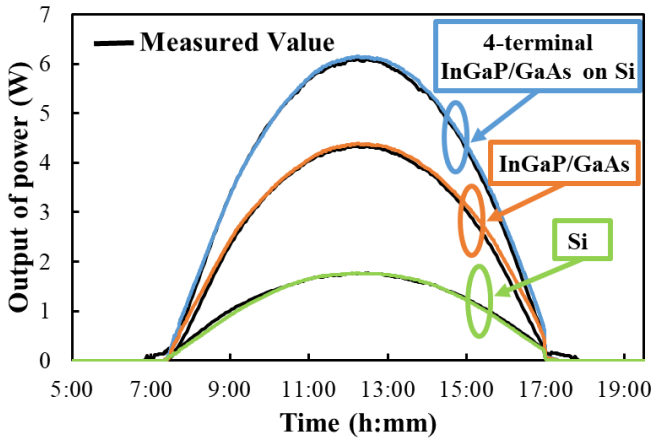

Figure 5. Validation of the performance model (MS2E model) to 4T tandem module, decomposing performance in each output terminal (InGaP/GaAs top cell, and Si bottom cell).

Table 1. Comparison between measured and estimated (predicted by MS2E model) energy yield in a day (January 3, 2019)

	Measured	Estimated	Error
InGaP/GaAs on Si[1]	39.6 Wh	40.4 Wh	1.9 %
InGaP/GaAs	28.0 Wh	28.9 Wh	3.4 %
Si	11.6 Wh	11.4 Wh	1.9 %

[1] 4T configuration independently takes the output from the top and bottom cells; the output of the InGaP/GaAs on Si module is a simple sum from the InGaP/GaAs top layer and Si bottom layer.

Preprints (www.preprints.org) | NOT PEER-REVIEWED | Posted: 2 March 2020 doi:10.20944/preprints202003.0028.v1

4. Discussion

It was shown that our MS2E model is sufficiently accurate to discuss the annual and outdoor performance of 4T tandem modules. Next, let us discuss and compare with other types of tandem modules with consideration of regional variations.

4.1. Comparison between 4T and 2T configuration

The annual performance of the 4T tandem module was calculated by the validated MS2E model. For comparison robustness to the seasonal spectrum change, it is essential to introduce a normalized scale of the performance, because the area, nominal output, cell type, and power conversion efficiency are different. We used performance ratio *PR* and the ratio of the performance peak-to-peak R_{pp} that is defined by Equation (3) and Equation (4).

$$PR = \frac{(Outdoor\ efficiency)}{(Efficiency\ measured\ by\ STC)} \tag{3}$$

$$R_{pp} = 1 - \frac{(peak\ to\ peak\ of\ PR\ in\ 4T)}{(peak\ to\ peak\ of\ PR\ in\ 2T)} \tag{4}$$

Note STC means the standard testing condition. *PR* value given by Equation (3) corresponds to how much power generation performance of the photovoltaic module drops in outdoor operation about the indoor testing result measured by the standard testing condition. R_{pp} value given by Equation (4) corresponds to the degree of suppression of the seasonal variation of performance of 4T configuration relative to standard 2T configuration. Both *PR* and R_{pp} values were integrated throughout a day, and their daily trend was plotted in time-series. The result with contrast to 2T configuration is shown in Figure 6 and Table 2. Note that the peak-to-peak value of the *PR* variation of 4T configuration was 0.084, and that of 2T was 0.139. The degree of improvement of seasonal variation R_{pp} was 39.8 % (Figure 6 (a)). As a result, the annual energy yield per nominal power of 4T configuration increased to 1500 kWh/kW, and that of 2T was 1442 kWh/kW (Table 2). The improvement was mainly seen in the summer. It corresponded to the variation of water precipitation (Figure 6 (b)). The bandgap of the bottom cell of Si is 1.11 eV, and the absorption edge is 1100 nm so that the performance of the Si bottom cell would not be affected by the water absorption typically seen in around 1200 nm.

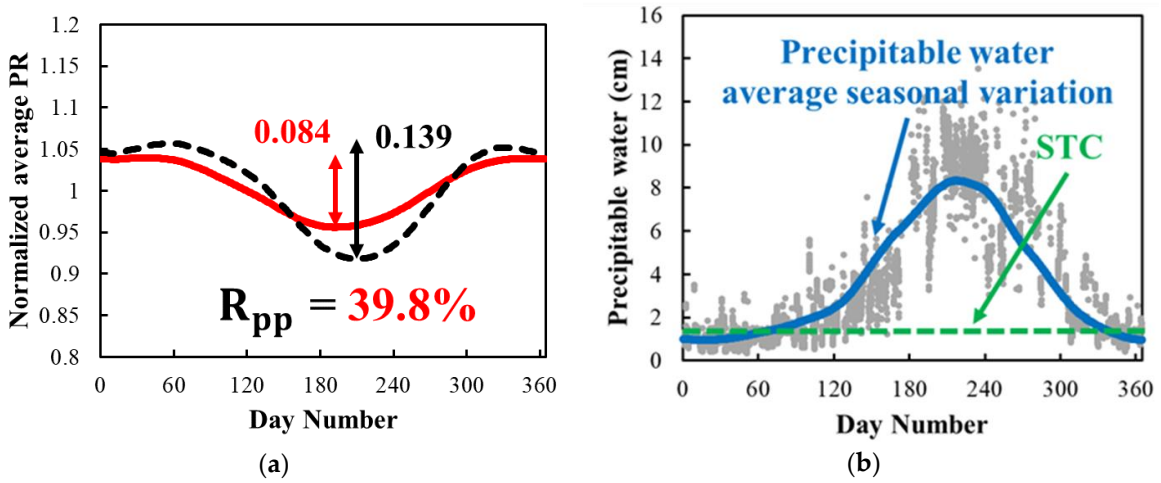

Figure 6. Comparison of the seasonal output between 4T configuration and 2T configuration affected by variation of the atmospheric parameter: (**a**) Predicted seasonal fluctuation of the normalized energy yield of 4T (red and solid line) and 2T (black and dashed line) configuration; (**b**) Seasonal variation of precipitable water (optical depth) in our measurement that is likely to be responsible from the difference of behavior between 2T and 4T configuration [38].

Table 2. This is a table. Tables should be placed in the main text near to the first time they are cited.

Preprints (www.preprints.org) | NOT PEER-REVIEWED | Posted: 2 March 2020 doi:10.20944/preprints202003.0028.v1

	PR peak to peak value	Annual energy yields (kWh/kW)
InGaP/GaAs on Si[1] (4-terminal configuration)	**0.084**	**1500**
InGaP/GaAs/InGaAs (2-terminal configuration)	**0.139**	**1442**

[1] 4T configuration independently takes the output from the top and bottom cells; the output of the InGaP/GaAs on Si module is a simple sum from the InGaP/GaAs top layer and Si bottom layer.

On the other hand, InGaAs bottom cell with 1.0 eV bandgap is affected by the absorption of this band. In 2T configuration, the reduction of absorbed photons in this water band constrains the current output of series-connected entire junctions. In addition to the difference in numbers of terminals (4T or 2T), the difference of the bandgap of the bottom cell affected the degree of the seasonal variation.

4.2. Regional difference in the behavior of 4T and 2T performance

The fact that the seasonal variation is affected by water precipitation implies that the gain by 4T configuration may be strongly affected by the local climate.

With the validation of the MS2E model in the estimation of PV output, we applied it more broadly. The solar database METPV-11 [45, 46] has solar irradiance measurement data for 837 locations in Japan. Using these data and our PV output forecasting model, we examined the seasonal energy yields in various locations with different climates. To determine the atmospheric parameters, measurement data of the solar spectrum are required. NEDO classified Japan into five solar radiation climate zones to clarify regional differences in solar radiation conditions. The solar spectrum was measured at five points, including Naganuma (Subarctic zone), Tosu (Temperate zone), and Okinoerabu (Subtropical zone). We extracted aerosol density and water precipitation in each solar radiation climate zone. Correctly, the aerosol density and water precipitation were extracted using a model in Equation (1) and (2) that minimizes the deviation of the global spectrum between the experimental values measured and the values. Note that the estimated global spectrum is a function of the variables aerosol density and water precipitation [38].

The result is shown in Figure 7. From left to right column, transition from the subarctic zone, temperate zone and subtropical zone, water precipitation, that were calculated by optical absorption of the spectrum using the method as mentioned above, increased. The gain of 4T configuration (R_{pp} value) increased accordingly.

Preprints (www.preprints.org) | NOT PEER-REVIEWED | Posted: 2 March 2020 doi:10.20944/preprints202003.0028.v1

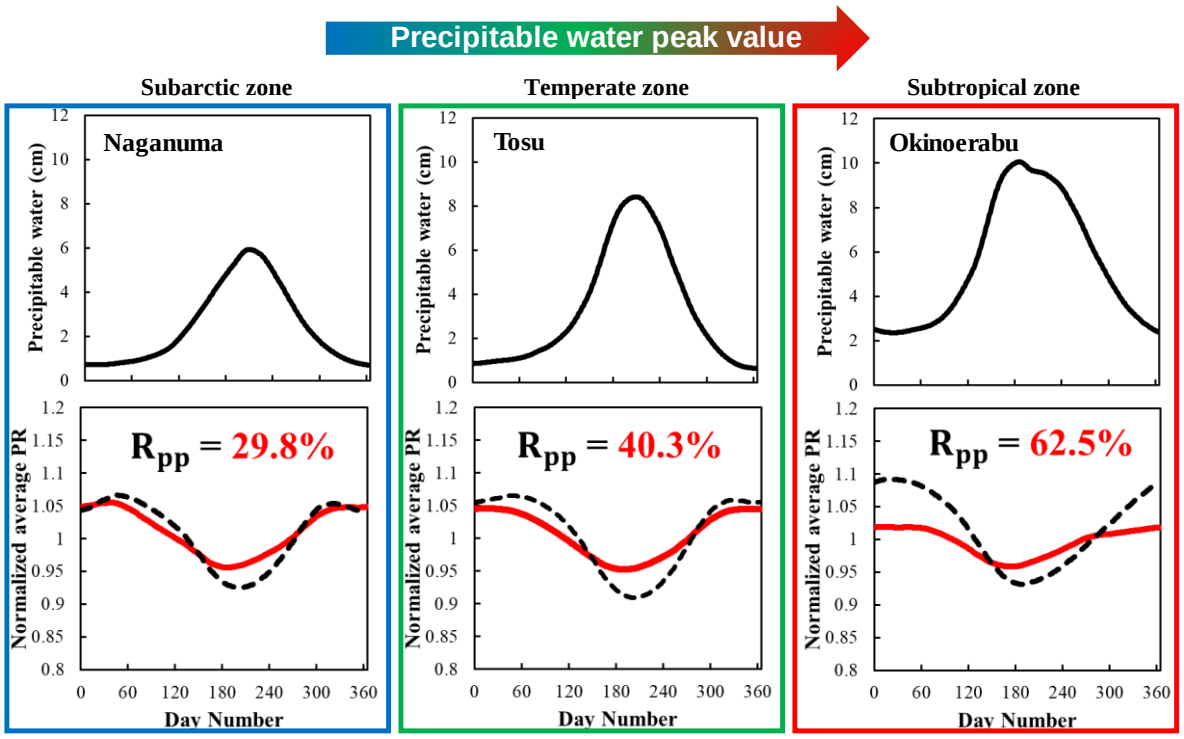

Figure 7. Comparison of the annual output between 4T configuration and 2T configuration affected by the variation of the atmospheric parameter. The red solid trend line in the bottom charts corresponds to the normalized energy yield of 4T, and the black dashed trend line corresponds to that of 2T configuration.

4.3.Further performance improvement

Although the 4T configuration effectively improves the seasonal loss of multi-junction modules, there still is some seasonal drop. It is because the top cell has two junctions, and its spectrum mismatching drops the output of the top cell.

Further improvement of the mismatching was proposed in several articles. One is fine-tuning of the bandgap energy [47]. The second is enhancing radiative coupling that was shown in the concentrator PV application [48] and non-concentrating application [1].

5. Conclusions

The advantage of the 4-terminal configuration of the photovoltaic module using a triple-junction solar cell, precisely, InGaP/GaAs on Si solar cell, was compared by conventional 2-terminal triple-junction module, specifically, InGaP/GaAs/InGaAs solar cell. The behavior of seasonal variation of performance and spectrum influence was modeled and validated outdoor measurement. The annual amplitude of the seasonal peak-to-peak performance ratio improved by about 40 %. This robust performance of the seasonal fluctuation of the solar spectrum is useful to applications to high-performance photovoltaic applications like zero-emission buildings and light-weight aerospace [49]. For the application to the vehicle-integrated photovoltaic, it is also essential to consider 3D Solar Irradiance (modeling [50] and measurement [51]), as well as the performance of the photovoltaic in the curved surface (modeling [52] and the standard [53]).

The seasonal fluctuation of the 2-terminal triple-junction solar is also responsible for seasonal variation of the water precipitation. The above-validated model was expanded to various climate zones. The advantage of 4T on Si configuration increases (subarctic zone) < (temperate zone) < (subtropical zone).

Author Contributions: Conceptualization: Y.O., and K.A.; methodology: H.T., H.S., Y.O., and K.A.; validation: H.T., H.S., T.T., Y.O., and K.A.; formal analysis: H.T., H.S., and Y.O.; data curation, H.T., H.S., and Y.O.; writing—

original draft preparation, H.T., K.A. and Y.O.; writing—review and editing: H.T., Y.O., and K.A.; supervision: K.N. and M.Y. All authors have read and agreed to the published version of the manuscript.

Funding: This research was funded by the New Energy and Industrial Technology Development Organization (NEDO), and a grant for Scientific Research on Priority Areas from the University of Miyazaki.

Acknowledgments: This work was supported in part by the New Energy and Industrial Technology Development Organization (NEDO).

Conflicts of Interest: The authors declare that there are no conflicts of interest.

References

1. Araki, K.; Ota, Y.; Saiki, H.; Tawa, H.; Nishioka, K.; Yamaguchi, M. Super-Multi-Junction Solar Cells—Device Configuration with the Potential for More Than 50% Annual Energy Conversion Efficiency (Non-Concentration). *Appl. Sci*. **2019**, *9*, 4598.
2. Ekins-Daukes, N.J.; Betts, T.R.; Kemmoku, Y.; Araki, K.; Lee, H.S.; Gottschalg, R.; Boreland, M.B.; Infield, D.G.; Yamaguchi, M. Syracuse-a multi-junction concentrator system computer model. In Proceedings of the Conference Record of the Thirty-First IEEE Photovoltaic Specialists Conference, Lake Buena Vista, FL, USA, 3–7 January 2005; pp. 651–654.
3. Cameron, C.; Crawford, C.; Foresi, J.; King, D.; McConnell, R.; Riley, D.; Sahm, A.; Stein, J. Performance Model Assessment for Multi-Junction Concentrating Photovoltaic Systems. *Aip Conf. Proc.* **2010**, *1277*, 290–293.
4. Araki, K; Yamaguchi, M. Influences of spectrum change to 3-junction concentrator cells. *Solar energy materials and solar cells*. *2003* Feb *1;75(3-4)*:707-14.
5. Cai, Y.; Wang, W.W.; Liu, C.W.; Ding, W.T.; Liu, D.; Zhao, F.Y. Performance evaluation of a thermoelectric ventilation system driven by the concentrated photovoltaic thermoelectric generators for green building operations. *Renew. Energy* **2020**, *147*, 1565–1583.
6. Richter, A.; Hermle, M.; Glunz, S.W. Reassessment of the limiting efficiency for crystalline silicon solar cells. *IEEE Journal of Photovoltaics* **2013**, *3*, 1184–1191.
7. Jackson, E.D. Areas for Improving of the Semiconductor Solar Energy Converter. In Proceedings of the Transzation Conference on the Use of Solar Energy, Tucson, AZ, USA, 31 October–1 November 1955; University of Arizona Press: Tucson, AZ, USA, 1958; Volume 5, pp. 122–126.
8. Wolf, M. Limitations and possibilities for improvement of photovoltaic solar energy converters. *Proc. Inst. Radio Eng*. **1960**, *48*, 1246–1263.
9. Hutchby, J.A.; Markunas, R.J.; Timmons, M.L.; Chiang, P.K.; Bedair, S.M. A Review of Multijunction Concentrator Solar Cells. In Proceedings of the 18th IEEE Photovoltaic Specialists Conference, Las Vegas, NV, USA, 21–25 October 1985; IEEE: New York, NY, USA, 1985; pp. 20–27.
10. Ludowise, M.J.; LaRue, R.A.; Borden, P.G.; Gregory, P.E.; Dietz, W.T. High-efficiency organometallic vapor phase epitaxy AlGaAs/GaAs monolithic cascade solar cell using metal interconnects. *Appl. Phys. Lett.* **1982**, *41*, 550–552.
11. Flores, C. A three-terminal double junction GaAs/GaAlAs cascade solar cells. *IEEE Electron. Device Lett.* **1983**, EDL–4, 96–99.
12. Chung, B.C.; Virshup, G.F.; Hikido, S.; Kaminar, N.R. 27.6% efficiency (1 Sun, air mass 1.5) monolithic Al0.37 Ga0.63 As/GaAs two-junction cascade solar cell with prismatic cover glass. *Appl. Phys. Lett.* **1989**, *55*, 1741–1743.
13. Fan, J.C.C.; Tsaur, B.Y.; Palm, B.J. Optical Design of High-Efficiency Multi-Junction Cells. In Proceedings of the 16th IEEE Photovoltaic Specialists Conference, San Diego, CA, USA, 27–30 September 1982; IEEE: New York, NY, USA, 1982; pp. 692–701.
14. Yamaguchi, M.; Amano, C.; Sugiura, H.; Yamamoto, A. High efficiency AlGaAs/GaAs multi-junction solar cells. In Proceedings of the 19th IEEE Photovoltaic Specialists Conference, New Orleans, LA, USA, 4–8 May 1987; IEEE: New York, NY, USA, 1987; pp. 1484–1485.
15. Ando, K.; Amano, C.; Sugiura, H.; Yamaguchi, M.; Saletesm, A. Non-radiative e-h recombination characteristics of mid-gap electron trap in AlxGa1–x As (x = 0.4) grown by molecular beam epitaxy. *Jpn. J. Appl. Phys.* **1987**, *26*, L266–L269.
16. Sugiura, H.; Amano, C.; Yamamoto, A.; Yamaguchi, M. Double hetero¬structure GaAs tunnel junction for AlGaAs/GaAs multi-junction solar cells. *Jpn. J. Appl. Phys.* **1988**, *27*, 269–272.

17. Olson, J.M.; Kurtz, S.R.; Kibbler, A.E. A 27.3% efficient Ga0.5In0.5P/ GaAs multi-junction solar cell. *Appl. Phys. Lett.* **1990**, *56*, 623–625.
18. Bertness, K.A.; Kurtz, S.R.; Friedman, D.J.; Kibbler, A.E.; Kramer, C.; Olson, J.M. 29.5%-efficiency GaInP/GaAs multi-junction solar cells. *Appl. Phys. Lett.* **1994**, *65*, 989–991.
19. Sasaki, K.; Agui, T.; Nakaido, K.; Takahashi, N.; Onitsuka, R.; Takamoto, T. Development of InGaP/GaAs/InGaAs inverted triple junction concentrator solar cells. *Aip Conf. Proc.* **2013**, *1556*, 22–25.
20. Chiu, P.T.; Law, D.L.; Woo, R.L.; Singer, S.; Bhusari, D.; Hong, W.D.; Zakaria, A.; Boisvert, J.C.; Mesropian, S.; King, R.R.; et al. 35.8% space and 38.8% terrestrial 5J direct bonded cells. In Proceedings of the 40th IEEE Photovoltaic Specialist Conference, Denver, CO, USA, 8–13 June 2014; pp. 11–13.
21. Yamaguchi, M.; Lee, K.-H. ;Araki, K.; and Kojima, N. *J. Phys. D. Appl. Phys.* **2018**, *51*, 133002.
22. Essig, S.; Allebe, C.; Remo, T.; Geisz, T. F.; Steiner, M. A.; Horowitz, K.; Barrud, L.; Ward, J. S.; Schnabel, M.; Descoeudres, A.; Young, D. L.; Woodhouse, M.; Despeisse, M.; Ballif, C.; Tamboli, A. Raising the one-sun conversion efficiency of III–V/Si solar cells to 32.8% for two junctions and 35.9% for three junctions. *Nat. Energy*, **2017**, *2*, 17144.
23. Green, M. A.; Dunlop, E. D.; Levi, D. H.; Hohl-Ebinger, J.; Yoshita, M.; Ho-Baillie, A. W. Y. Solar cell efficiency tables (version 54). *Prog. Photovoltaics* **2019**, *27*, 565.
24. Carmody, M.; Mallick, S.; Margetis, J.; Kodama, R.; Biegala, T.; Xu, D.; Bechmann, P.; Garland, J. W.; Sivananthan, S. Single-crystal II-VI on Si single-junction and tandem solar cells. *Appl. Phys. Lett.* **2010**, *96*, 153502.
25. Yao, M.; Cong, S.; Arab, S.; Huang, N.; Povinelli, M. L.; Cronin, S. B.; Dapkus, P. D.; Zhou, C. Tandem solar cells using GaAs nanowires on Si: design, fabrication, and observation of voltage addition. *Nano Lett.* **2015**, *15*, 7217.
26. Araki. K.; Ota, Y.; Lee, KH.; Nishioka, K.; Yamaguchi, M. Is it CPV? Yes, but it is a partial CPV. In AIP Conference Proceedings 2017 Sep 6 (Vol. 1881, No. 1, p. 080001). AIP Publishing LLC.
27. Araki, K.; Lee, KH.; Yamaguchi, M. The possibility of the static LCPV to mechanical-stack III-V//Si module. InAIP Conference Proceedings 2018 Sep 13 (Vol. 2012, No. 1, p. 090002). AIP Publishing LLC.
28. Sato, D.; Lee, KH.; Araki, K.; Masuda, T.; Yamaguchi, M.; Yamada, N. Design and Evaluation of Low-concentration Static III-V/Si Partial CPV Module for Car-rooftop Application. In2018 IEEE 7th World Conference on Photovoltaic Energy Conversion (WCPEC)(A Joint Conference of 45th IEEE PVSC, 28th PVSEC & 34th EU PVSEC) 2018 Jun 10 (pp. 0954-0957). IEEE.
29. Takamoto, T.; Washio, H.; Juso, H. Application of InGaP/GaAs/InGaAs triple junction solar cells to space use and concentrator photovoltaic. In Proceedings of the 2014 IEEE 40th Photovoltaic Specialist Conference (PVSC), Denver, CO, USA, 8–13 June 2014; pp. 1–5.
30. Ishii, T.; Otani, K.; Takashima, T.; Xue, Y. Solar spectral influence on the performance of photovoltaic (pv) modules under fine weather and cloudy weather conditions. Prog. Photovoltaics 2013, 21, 481–489.
31. Araki, K.; Yamaguchi, M. Influences of spectrum change to 3-junction concentrator cells. *Sol. Energy Mater. Sol. Cells* **2003**, *75*, 707–714.
32. Faine, P.; Kurtz, S.R.; Riordan, C.; Olson, J.M. The influence of spectral solar irradiance variations on the performance of selected single-junction and multijunction solar cells. *Solar Cells* **1991**, *31*, 259–278.
33. Kirn, B.; Topic, M. Diffuse and direct light solar spectra modeling in pv module performance rating. *Sol. Energy* **2017**, *150*, 310–316.
34. Nofuentes, G.; García-Domingo, B.; Muñoz, J.V.; Chenlo, F. Analysis of the dependence of the spectral factor of some pv technologies on the solar spectrum distribution. *Appl. Energy* **2014**, *113*, 302–309.
35. Alonso-Abella, M.; Chenlo, F.; Nofuentes, G.; Torres-Ramírez, M. Analysis of spectral effects on the energy yield of different pv (photovoltaic) technologies: The case of four specific sites. *Energy* **2014**, *67*, 435–443.
36. Cariou, R.; Benick, J.; Feldmann, F.; Höhn, O.; Hauser, H.; Beutel, P.; Razek, N.; Wimplinger, M.; Bläsi, B.; Lackner, D.; Hermle, M.; Siefer, G.; Glunz, S.W.; Bett, A.W.; Dimroth, F. III–V-on-silicon solar cells reaching 33% photoconversion efficiency in two-terminal configuration. *Nature Energy* **2018**, *3*, 326-333
37. Bird, R.E.; Riordan, C. Simple solar spectral model for direct and diffuse irradiance on horizontal and tilted planes at the earth's surface for cloudless atmospheres. *Journal of Climate & Applied Meteorology* **1986**, *25*, 87–97.
38. Tawa, H.; Saiki, H.; Ota, Y.; Araki, K.; Takamoto, T.; Nishioka, K. Accurate Output Forecasting Method for Various Photovoltaic Modules Considering Incident Angle and Spectral Change Owing to Atmospheric Parameters and Cloud Conditions. *Appl. Sci.* **2020**, *10*, 703.

39. Araki, K.; Ota, Y.; Sakai, T.; Lee, K.H.; Nishioka, K.; Yamaguchi, M. Energy yield prediction of multi-junction cells considering atmospheric parameters fluctuation using Monte Carlo methods. In Proceedings of the PVSEC-27, Otsu, Japan, 12–17 November 2017.
40. Araki, K.; Ota, Y.; Sakai, T.; Lee, K.H.; Yamaguchi, M. Inherent uncertainty of energy ratings of multi-junction cells by the fluctuation of atmospheric parameters. In Proceedings of the PVSEC-27, Otsu, Japan, 12–17 November 2017.
41. Araki K, Ota Y, Lee KH, Sakai T, Nishioka K, Yamaguchi M. Analysis of fluctuation of atmospheric parameters and its impact on performance of CPV. InAIP Conference Proceedings 2018 Sep 13 (Vol. 2012, No. 1, p. 080002). AIP Publishing LLC.
42. Araki K, Yamaguchi M, Takamoto T, Ikeda E, Agui T, Kurita H, Takahashi K, Unno T. Characteristics of GaAs-based concentrator cells. Solar energy materials and solar cells. 2001 Feb 1;66(1-4):559-65.
43. Araki K, Yamaguchi M. Extended distributed model for analysis of non-ideal concentration operation. Solar energy materials and solar cells. 2003 Feb 1;75(3-4):467-73.
44. Saiki H, Sakai T, Araki K, Ota Y, Lee KH, Yamaguchi M, Nishioka K. Verification of uncertainty in CPV's outdoor performance. In2018 IEEE 7th World Conference on Photovoltaic Energy Conversion (WCPEC)(A Joint Conference of 45th IEEE PVSC, 28th PVSEC & 34th EU PVSEC) 2018 Jun 10 (pp. 0949-0953). IEEE.
45. Itagaki, A.; Okumura, H.; Yamada, A. Preparation of meteorological data set throughout Japan for suitable design of PV systems Photovoltaic Energy Conversion. In Proceedings of the 3rd World Conference on Photovoltaic Energy Conversion, Osaka, Japan, 11–18 May 2003; Volume 2. [Google Scholar]
46. Shirakawa, K.; Itagaki, A.; Utsunomiya, T. Preparation of hourly solar radiation data on inclined surface (METPV-11) throughout Japan. In Proceedings of the JSES/JWEA Joint Conference, Wakkanai, Japan, 21–22 September 2011; pp. 193–196.
47. Araki K, Ota Y, Lee KH, Nishioka K, Yamaguchi M. Improvement of the spectral sensitivity of CPV by enhancing luminescence coupling and fine-tuning to the bottom-bandgap matched to local atmospheric conditions. InAIP Conference Proceedings 2019 Aug 26 (Vol. 2149, No. 1, p. 060001). AIP Publishing LLC.
48. Araki K, Ota Y, Lee KH, Nishioka K, Yamaguchi M. Super-Multi-Junction Solar Cells, a New Configuration of the Robust and High-Efficiency Solar Cell and Its Application–Operation Model Based on the Annual Monitoring of the Multi-Junction PV Modules. In2019 18th International Conference on Optical Communications and Networks (ICOCN) 2019 Aug 5 (pp. 1-3). IEEE.
49. Araki, K.; Ji, L.; Kelly, G.; Yamaguchi, M. To Do List for Research and Development and International Standardization to Achieve the Goal of Running a Majority of Electric Vehicles on Solar Energy. Coatings 2018, 8, 251.
50. Araki, K.; Ota, Y.; Yamaguchi, M. Measurement and Modeling of 3D Solar Irradiance for Vehicle-Integrated Photovoltaic. Appl. Sci. 2020, 10, 872.
51. Ota Y, Masuda T, Araki K, Yamaguchi M. A mobile multipyranometer array for the assessment of solar irradiance incident on a photovoltaic-powered vehicle. Solar Energy. 2019 May 15;184:84-90.
52. Ota Y, Masuda T, Araki K, Yamaguchi M. Curve-correction factor for characterization of the output of a three-dimensional curved photovoltaic module on a car roof. Coatings. 2018 Dec;8(12):432.
53. Tayagaki T, Araki K, Yamaguchi M, Sugaya T. Impact of Nonplanar Panels on Photovoltaic Power Generation in the Case of Vehicles. IEEE Journal of Photovoltaics. 2019 Sep 23;9(6):1721-6.
54. Araki K, Algora C, Siefer G, Nishioka K, Leutz R, Carter S, Wang S, Askins S, Ji L, Kelly G. Standardization of the CPV and Car-roof PV Technology in 2018–Where are We Going to Go?. InAIP Conference Proceedings 2018 Sep 13 (Vol. 2012, No. 1, p. 070001). AIP Publishing LLC.